Crystal phase-controlled synthesis of rod-shaped AgInTe$_2$ nanocrystals for *in vivo* imaging in the near-infrared wavelength region†

Tatsuya Kameyama,[a] Yujiro Ishigami,[a] Hiroshi Yukawa,[a,b] Taisuke Shimada,[a] Yoshinobu Baba,[a,b,c] Tetsuya Ishikawa,[d] Susumu Kuwabata[e] and Tsukasa Torimoto*[a]

Rod-shaped AgInTe$_2$ nanocrystals (NCs) exhibiting intense near-band edge photoluminescence in the near-infrared (NIR) wavelength region, were successfully prepared by the thermal reaction of metal acetates and Te precursors in 1-dodecanethiol. Increasing the reaction temperature resulted in the formation of larger AgInTe$_2$ NCs with crystal structures varying from hexagonal to tetragonal at reaction temperatures of 280 °C or higher. The energy gap was increased from 1.13 to 1.20 eV with a decrease in rod width from 8.3 to 5.6 nm, accompanied by a blue shift in the photoluminescence (PL) peak wavelength from 1097 to 1033 nm. The optimal PL quantum yield was approximately 18% for AgInTe$_2$ NCs with rod widths of 5.6 nm. The applicability of AgInTe$_2$ NCs as a NIR-emitting material for *in vivo* biological imaging was examined by injecting AgInTe$_2$ NC-incorporated liposomes into the back of a C57BL/6 mouse, followed by *in vivo* photoluminescence imaging in the NIR region.

Colloidal semiconductor nanocrystals (NCs) with absorbing and emitting properties in the near-infrared (NIR) light region have attracted considerable attention because of their potential applications in biological imaging,[1–7] sensors,[8,9] and solar energy conversion systems.[4–6,9–14] NIR light penetrates more efficiently into biological tissues such as skin and blood than light in the ultraviolet, visible, and IR wavelength regions; thus making them promising probes for biological applications, particularly for *in vivo* imaging.[15–18] To this end, many studies have attempted to develop NIR light-emitting semiconductor

nanocrystals as photoluminescent markers, because they exhibited unique and excellent physicochemical properties, including a broad absorption band, size-tunable photoluminescence (PL) peak, and high PL quantum yield (QY), in comparison with other NIR light-emitting materials such as organic dyes or lanthanide-based upconversion nanoparticles.[1–3,7]

To date, high-quality semiconductor NCs that exhibit NIR photoluminescence, such as CdTe,[19,20] PbS,[21] and PbSe,[22] have been prepared *via* solution syntheses. *In vivo* imaging has been successfully conducted by the surface modification of NCs with bifunctional agents containing hydrophilic functional groups or by the incorporation of NCs into liposomes or micelles. Furthermore, nanocrystals not containing toxic metal elements such as Ag$_2$S,[20,23] Ag$_2$Se,[24] AgInS$_2$,[20,25] and CuInS$_2$[5,26,27] have been reported to show intense PL in the NIR region. For example, binary semiconductors of Ag$_2$S and Ag$_2$Se with band gaps of 1.0 and 0.15 eV, respectively, have been utilized as NIR-emitting markers *in vivo*. Hocaoglu *et al.* successfully prepared highly photoluminescent Ag$_2$S NCs (PL QY < 39%) that showed good cytocompatibility using NIH/3T3 cell lines.[23] Wang *et al.* demonstrated the *in vivo* imaging of vascular structures of mice using Ag$_2$Se NCs with a PL QY of 29%.[24] Since an AgInTe$_2$ semiconductor was reported to have a bulk band gap of approximately 1.0 eV,[28] size-controlled AgInTe$_2$ NCs show promise as NIR light-emitting markers in the second NIR window at wavelengths of 1000–1350 nm, in which the signal-to-noise ratios of *in vivo* PL imaging are much more improved than those in the first NIR window with wavelengths from 700 to 900 nm, because of reduced photon absorption and lower autofluorescence by biological tissues.[16,29] However, with the exception of the recent preparation of spherical, approximately 10.6 nm AgInTe$_2$ NCs that exhibited a low PL QY of 0.06%,[30] no attempts have been made to fabricate highly photoluminescent AgInTe$_2$ NCs with sizes less than several tens of nanometers. Moreover, such AgInTe$_2$ NCs have never been successfully applied to *in vivo* biological imaging because of their low QY of NIR photoluminescence.

Here, we report rod-shaped AgInTe$_2$ NCs with controlled widths and lengths. The obtained NCs exhibit intense PL and

[a]*Graduate School of Engineering, Nagoya University, Furo-cho, Chikusa-ku, Nagoya 464-8603, Japan. E-mail: torimoto@apchem.nagoya-u.ac.jp*
[b]*ImPACT Research Center for Advanced Nanobiodevices, Nagoya University, Furo-cho, Chikusa-ku, Nagoya 464-8603, Japan*
[c]*Institute of Innovation for Future Society, Nagoya University, Furo-cho, Chikusa-ku, Nagoya 464-8603, Japan*
[d]*Department of Medical Laboratory Sciences, Graduate School of Medicine, Nagoya University, Daikominami, Higashi-ku, Nagoya 461-8673, Japan*
[e]*Graduate School of Engineering, Osaka University, 2-1 Yamada-oka, Suita, Osaka 565-0871, Japan*
†Electronic supplementary information (ESI) available: A detailed synthesis procedure of DSPC-AgInTe$_2$ and analytical data of AgInTe$_2$ NCs. See DOI: 10.1039/c5nr07532g

the peak wavelength in the NIR region is tunable by changing the rod width, enabling their use as an NIR marker for *in vivo* biological imaging.

AgInTe$_2$ NCs were prepared through the thermal reaction of metal acetates and Te in a hot organic solvent. Elemental Te powder (10.7 mmol) and trioctylphosphine (30 cm^3) were loaded in a three-neck flask under vacuum and then heated to 80 °C under vigorous stirring. The flask was then purged with N$_2$ and heated to 240 °C for 3 h, yielding a clear orange solution. The obtained Te precursor solution was cooled to room temperature and stored under an N$_2$ atmosphere. Powders of silver acetate (0.075 mmol) and indium acetate (0.075 mmol) were placed in a test tube with 3.0 cm^3 of 1-dodecanethiol followed by vigorous stirring under an N$_2$ atmosphere. A 0.42 cm^3 portion of the Te precursor solution containing 0.15 mmol of Te was injected into the solution, and the mixture was then immediately heat-treated at various temperatures (180 °C–300 °C) for 5 min with vigorous stirring under an N$_2$ atmosphere. The resulting suspension was subjected to centrifugation at 4000 rpm for 5 min to remove large particles. AgInTe$_2$ NCs were separated from the supernatant by the addition of 5 cm^3 ethanol. The obtained precipitate was isolated by centrifugation and washed twice with ethanol. Finally, the AgInTe$_2$ NCs were dissolved in octane for various characterizations. Detailed information about the characterization of the NCs is shown in the ESI.†

Fig. 1a shows the X-ray powder diffraction (XRD) patterns of the obtained nanocrystals prepared at 180 °C–300 °C. The particles prepared at temperatures of 280 °C or higher exhibited three predominant peaks at 2θ = 24.0°, 39.8°, and 46.8°, which were respectively assigned to the diffractions of the (112), (204), and (312) planes of tetragonal AgInTe$_2$ (Fig. 1b; PDF# 01-075-0119). In contrast, the XRD patterns of nanocrystals prepared at temperatures of 250 °C or lower did not match the previously reported patterns or standard ICDD (PDF-2) patterns of AgInTe$_2$ or other conceivable crystal phases such as

AgIn$_8$Te$_5$, Ag$_2$Te, and In$_2$Te$_3$. The hexagonal wurtzite crystal phase has been reported in the NCs of multinary semiconductors such as CuInS$_2$,[31] CuGaS$_2$,[32] and Cu$_2$ZnSnS$_4$[32] depending on the preparation conditions, even if the bulk crystals have predominantly tetragonal or cubic zinc-blende crystal structures. Thus, we simulated the XRD pattern of cation-disordered hexagonal AgInTe$_2$ (Fig. 1c) according to previously reported methods for CuInS$_2$,[31] in which the hexagonal crystal structure was considered to be a derivative of wurtzite ZnS in such a way that the metal ions of Cu and In randomly substituted the Zn site (see the ESI† for details). The simulated XRD pattern of cation-disordered wurtzite AgInTe$_2$ (the bottom of Fig. 1a) matched well with the patterns observed for the nanocrystals prepared at temperatures of 250 °C or lower. It should be noted that peaks at 23°, 26°, and 43° assignable to hexagonal AgInTe$_2$ were still detected in the XRD pattern (iv) of particles prepared at 280 °C shown in Fig. 1a but their intensities were much smaller than those assigned to tetragonal AgInTe$_2$, indicating that the phase transition of most AgInTe$_2$ nanoparticles from the hexagonal to tetragonal structure was completed within a relatively narrow temperature range between 250 and 280 °C.

Elemental analysis revealed that the obtained AgInTe$_2$ NCs had nearly stoichiometric chemical compositions, irrespective of reaction temperature (Fig. S1†), although slightly In-rich and Ag-deficient compositions were detected in the nanocrystals prepared at temperatures of 250 °C or lower. These results suggested that the AgInTe$_2$ NCs prepared in this study contained small amounts of crystal defects such as Ag vacancies, interstitial In, and/or antisite defects of In$_{Ag}$. Fig. 2a–c show representative TEM images of the AgInTe$_2$ NCs formed at 180 °C, 250 °C, and 300 °C (images of NCs obtained at other temperatures are shown in Fig. S2†). Rod-like particles were formed, and their sizes increased slightly with increasing formation temperature. As shown in Fig. 2d, the average width of
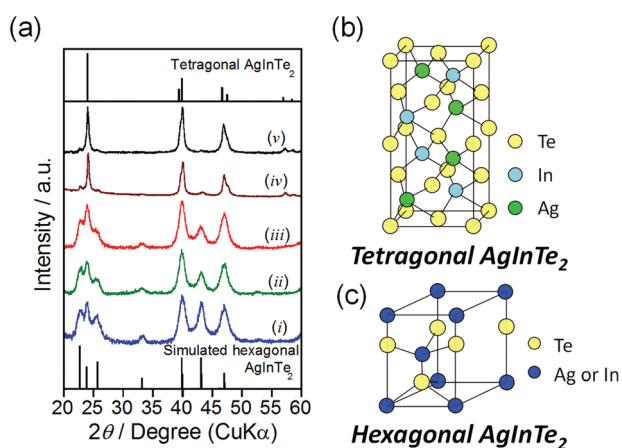

Fig. 1 (a) XRD patterns of AgInTe$_2$ NCs prepared at various temperatures; (i) 180 °C, (ii) 220 °C, (iii) 250 °C, (iv) 280 °C, and (v) 300 °C. Schematic illustration of unit cells of AgInTe$_2$ with tetragonal (b) and hexagonal crystal structures (c).
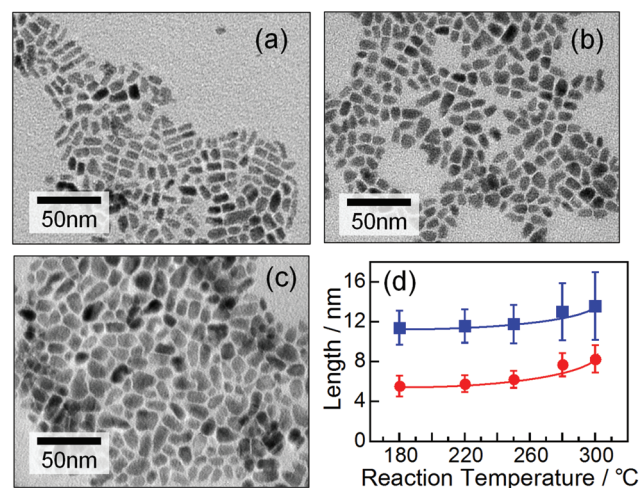

Fig. 2 Representative TEM images of AgInTe$_2$ NCs prepared at (a) 180 °C, (b) 250 °C, and (c) 300 °C. (d) Dependences of width (circles) and length (squares) of AgInTe$_2$ NCs on the temperature in preparation.

the particles increased monotonically from 5.5 to 8.3 nm with increasing reaction temperature from 180 °C to 300 °C, accompanied by an increase in the average length from 11.4 to 13.5 nm. It should be noted that reaction temperatures higher than 280 °C induced the tetragonal crystal structure, produced a larger fraction of AgInTe$_2$ NCs with irregular non-rod shapes, and resulted in a wider size distribution.

The solutions containing AgInTe$_2$ NCs were deep-black in color due to strong light absorption in the visible and NIR wavelength regions, as observed in the absorption spectra shown in Fig. 3a. Irrespective of the synthetic temperature, an obscure absorption shoulder attributed to the exciton transition appeared at approximately 1000 nm with the absorption onset at approximately 1150–1200 nm. Relatively strong PL was observed in the NIR wavelength region for all AgInTe$_2$ NCs. The PL spectra (Fig. 3a) exhibited somewhat wide FWHMs of approximately 100–150 nm, corresponding to approximately 110–180 meV. Each PL peak was located near the corresponding absorption onset, and the peak wavelength was red-shifted, as expected from the enlargement in the width of AgInTe$_2$ NCs with increasing reaction temperature (Fig. 2d) as discussed below. Typical I–III–VI$_2$ semiconductor nanocrystals such as AgInS$_2$, AgInSe$_2$, and CuInS$_2$ have been reported to exhibit broad PL peaks (FWHM of approximately 200–400 meV)[33–35] in the visible-light region with a large Stokes shifts of >100 meV; in these cases, the PL was attributed to donor–acceptor pair recombination and/or emission from trap sites. In contrast, binary, NIR-emitting, high-quality semiconductor nanocrystals, such as CdTe and PbS, exhibited narrow near-band edge emissions with FWHMs of approximately 50–100 meV.[36,37] Considering these results, the PL of the AgInTe$_2$ NCs formed in the present study can likely be attributed to radiative emission from donor–acceptor levels near the band edge.

Fig. 3b shows the energy gap (E_g) obtained from the absorption onset, the PL peak energy (E_{PL}), and the PL QY as a function of AgInTe$_2$ NC width. Since the exciton peak was not clearly observed in the individual absorption spectra, a Tauc plot was adopted to determine the value of E_g (Fig. S3 in the ESI†). Both the E_g and E_{PL} increased with decreasing particle size. The exciton Bohr radius, a_B, of AgInTe$_2$ was calculated to be 3.5 nm from the dielectric constant of 6.48 (ref. 38) and the effective masses of electrons and holes of 0.108 and 1.012, respectively.[39] Since the quantum size effect appears when the NC size becomes smaller than $2a_B$, it is reasonable to assume that decreasing the AgInTe$_2$ NC width to smaller than approximately 7 nm enlarged both E_g and E_{PL} due to the quantum size effect.

The PL QY has been reported to be enhanced with decreasing size for various types of semiconductor nanocrystals, including CuInS$_2$,[40] CdS,[41] CdTe,[42] and Si.[43] These results were most likely due to the greater confinement of photogenerated electron–hole pairs in smaller-sized NCs, which increased the probability of radiative recombination. This can be true for the AgInTe$_2$ NCs in the current study, in which the PL QY was improved when the widths of the rod-shaped AgInTe$_2$ NCs decreased (Fig. 3b). The maximum PL QY of 18%, obtained in the present study for the hexagonal phase AgInTe$_2$ NCs 5.5 nm in width, was quite larger than that previously reported for spherical AgInTe$_2$ NCs having a relatively large diameter of 10.6 nm, 0.06%, probably because of the greater confinement of photogenerated carriers in smaller NCs. Although this value was approximately half of the PL QYs observed for conventional NIR-emissive semiconductor nanocrystals of PbS, Ag$_2$S, or Ag$_2$Se, it was comparable to that of indocyanine green, which is practically used as a dye for biological imaging.[44] Hence, the relatively intense NIR emission of the AgInTe$_2$ NCs demonstrates their potential use as an NIR marker for biological imaging.

The as-prepared AgInTe$_2$ NCs could not be uniformly dispersed in aqueous solutions because of their hydrophobic surface modified with 1-dodecanethiol (used as a stabilizing agent). This makes the direct injection of these NCs in biological tissues difficult. Therefore, in this study, small unilamellar liposomes of 1,2-distearoyl-*sn*-glycero-3-phosphocholine (DSPC; Fig. 4a) were utilized as carriers to transfer the AgInTe$_2$ NCs into aqueous solution without aggregation. A previously reported preparation method for DSPC liposomes containing hydrophilic CdSe NCs was employed.[45] The hexagonal AgInTe$_2$ NCs with a PL QY of 18% were incorporated into DSPC liposomes [see the ESI† for the detailed preparation procedure of the DSPC–AgInTe$_2$ NC nanocomposite (DSPC–AgInTe$_2$)]. Dynamic light scattering measurements revealed that the DSPC–AgInTe$_2$ composite particles had an average hydrodynamic diameter of 1.8×10^2 nm (Fig. S4†), in rough agreement with the previously reported value for DSPC–CdSe nanocomposites (approximately 1.7×10^2 nm).[45] The average number of AgInTe$_2$ NCs in an individual liposome was estimated to be 4.4×10^2 particles using the concentrations of DSPC and AgInTe$_2$ NCs and the molar absorption coefficient (ε) of AgInTe$_2$ NCs (Fig. S5†). We should note that the AgInTe$_2$ NCs exhibited relatively large ε values greater than approximately 10^5 dm^3 mol^{-1} (particles) cm^{-1} at incident photon energies
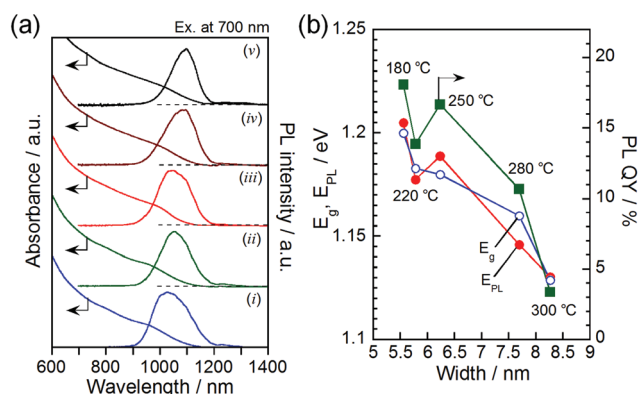

Fig. 3 (a) Absorption and PL spectra of AgInTe$_2$ NCs prepared at temperatures of (i) 180 °C, (ii) 220 °C, (iii) 250 °C, (iv) 280 °C, and (v) 300 °C. The wavelength of excitation light for PL measurement was 700 nm. (b) Plots of E_g, E_{PL}, or PL QY as a function of the width of AgInTe$_2$ NCs.
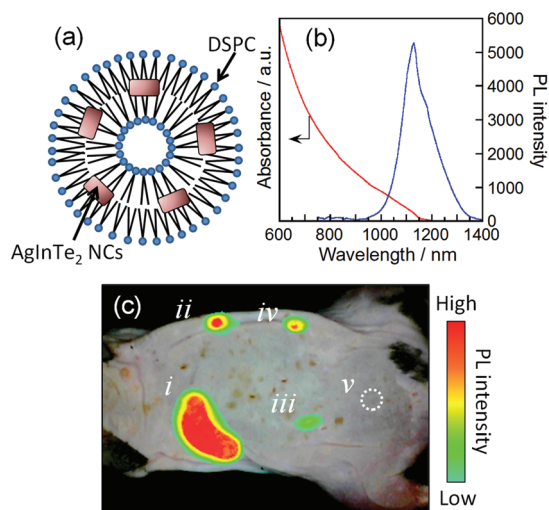
Fig. 4 (a) Schematic illustration of DSPC−AgInTe$_2$ NC composites and (b) their absorption and PL spectra. The wavelength of excitation light for PL measurement was 700 nm. (c) *In vivo* photoluminescence imaging of a mouse after injection of a 50 mm^3 portion of DSPC−AgInTe$_2$ dispersion. The concentrations of AgInTe$_2$ NCs injected in dispersion were 50 (i), 25 (ii), 12.5 (iii), 6.25 (iv), and 0 nmol (particles) dm^{-3} (v).

greater than approximately 1.1 eV. These ε values were comparable to those of conventional NIR-emissive PbS nanocrystals of 6.5 nm in average size (*ca.* 6×10^6 dm^3 mol^{-1} (particles) cm^{-1} at 3.1 eV).[46] Both the PL peak and the absorption onset of the AgInTe$_2$ NCs incorporated into DSPC liposomes were red shifted by 50–100 nm compared with those of the original particles (Fig. 4b); these red shifts were accompanied by a decrease in the PL QY from 18% to 2.2%. These results suggest that NC coalescence slightly occurred during the incorporation process. To utilize the thus prepared DSPC−AgInTe$_2$ NC composites for biological imaging, it is important to evaluate the durability of photoluminescent AgInTe$_2$ NCs under various environmental conditions.[47,48] We dispersed the DSPC−AgInTe$_2$ NC composites in 10 mmol dm^{-3} phosphate buffer solutions at different pH values (pH 5.4, 7.0, or 8.5) and monitored the changes in the PL intensity of AgInTe$_2$ NCs (Fig. S6†). The AgInTe$_2$ NCs exhibited an almost constant PL intensity for at least 24 h when a DSPC−AgInTe$_2$ NC composite solution at pH 7.0 was stored in the dark under an N$_2$ atmosphere. On the other hand, the PL intensities of AgInTe$_2$ NC solutions at both pH 7.0 and 5.4 gradually decreased in air with the elapse of time and finally reached *ca.* 85% of the initial values after 24 h, while the deterioration of the PL intensity in air was enhanced in a basic buffer solution at pH 8.5 where AgInTe$_2$ NCs exhibited *ca.* 20% of the initial PL intensity after 24 h. These results suggested that the ideal pH range of DSPC−AgInTe$_2$ NC composites as a PL probe was between pH 7.0 and 5.4. It should be noted that the continuous irradiation to the DSPC−AgInTe$_2$ NC composite solution (pH 7.0) in air by the excitation light with a wavelength of 700 nm (the intensity of 17.5 mW cm^{-2}) also induced the

remarkable deterioration of the PL peak probably due to the partial photooxidation of the AgInTe$_2$ NC surface, the intensity being 20% as small as the initial value after *ca.* 8 h.

As mentioned above, the obtained water-soluble DSPC−AgInTe$_2$ can emit in the NIR wavelength region. To explore the potential application of AgInTe$_2$ NCs for *in vivo* imaging, the DSPC−AgInTe$_2$ composites were injected into the back of a hair-removed C57BL/6 mouse after the dilution of the original composite dispersion containing 50 nmol (particles) dm^{-3} AgInTe$_2$ NCs with phosphate-buffered saline (pH 7.4). Fig. 4c shows an NIR PL image obtained using an SAI-1000 portable *in vivo* fluorescence imaging system (SHIMADZU; excitation laser, 980 nm; emission filter, 1080 nm long-pass). In Fig. 4c, the obtained PL image was superimposed on the photograph of the mouse. The NIR PL emitted from the AgInTe$_2$ NCs was clearly observed through the mouse skin, which was approximately 2 mm in thickness, even when the concentration of AgInTe$_2$ NCs in dispersion was as low as 6.25 nmol (particles) dm^{-3}. The NIR PL signals were detectable for 5 h after injection when the concentration was higher than 12.5 nmol (particles) dm^{-3}, although the PL intensity at the site of the injection of 12.5 nmol (particles) dm^{-3} AgInTe$_2$ NCs was approximately 30% as high as in the initial state (Fig. S7†).

Conclusions

In conclusion, size-quantized, rod-shaped AgInTe$_2$ NCs were prepared *via* the thermal reaction of metal acetates and Te precursors in 1-dodecanethiol. The widths and lengths of the NCs increased monotonically with increasing reaction temperature. Their crystal structures, either hexagonal or tetragonal, could be controlled by choosing the reaction temperature. The energy gap and PL peak position of the rod-shaped NCs were tunable and depended on the particle width. The highest intensity of near-band edge PL in the NIR region was obtained for the particles prepared at 180 °C (PL QY = 18%), demonstrating the applicability of the AgInTe$_2$ NCs as an efficient NIR-emitting marker for *in vivo* imaging. Since the surface coating of NCs, such as CdSe, CuInS$_2$ and AgInS$_2$, with a wider band gap semiconductor, such as ZnS and CdS, has been reported to enhance the stability of NCs and increase their PL QY several times greater than that without coating,[26,34,49] the fabrication of such core–shell structures with AgInTe$_2$ NCs as a core will be a useful strategy for further improving their performance as a biological marker. The findings of this study provide a new candidate for NIR-light-sensitive materials without highly toxic metal elements, such as Cd and Pb, for various optical applications, including *in vivo* biological imaging and solar energy conversion systems.

Acknowledgements

Notes and references

1 S. Kim, Y. T. Lim, E. G. Soltesz, A. M. De Grand, J. Lee, A. Nakayama, J. A. Parker, T. Mihaljevic, R. G. Laurence, D. M. Dor, L. H. Cohn, M. G. Bawendi and J. V. Frangioni, *Nat. Biotechnol.*, 2004, **22**, 93–97.

2 H. Yukawa, M. Watanabe, N. Kaji, Y. Okamoto, M. Tokeshi, Y. Miyamoto, H. Noguchi, Y. Baba and S. Hayashi, *Biomaterials*, 2012, **33**, 2177–2186.

3 S. E. Lohse and C. J. Murphy, *J. Am. Chem. Soc.*, 2012, **134**, 15607–15620.

4 H. Z. Zhong, Z. L. Bai and B. S. Zou, *J. Phys. Chem. Lett.*, 2012, **3**, 3167–3175.

5 J. Kolny-Olesiak and H. Weller, *ACS Appl. Mater. Interfaces*, 2013, **5**, 12221–12237.

6 S. V. Kershaw, A. S. Susha and A. L. Rogach, *Chem. Soc. Rev.*, 2013, **42**, 3033–3087.

7 J. Niu, X. Wang, J. Lv, Y. Li and B. Tang, *TrAC Trends Anal. Chem.*, 2014, **58**, 112–119.

8 Y. S. Xia, L. Song and C. Q. Zhu, *Anal. Chem.*, 2011, **83**, 1401–1407.

9 T. Torimoto, T. Kameyama and S. Kuwabata, *J. Phys. Chem. Lett.*, 2014, **5**, 336–347.

10 J. B. Sambur, T. Novet and B. A. Parkinson, *Science*, 2010, **330**, 63–66.

11 J. Jasieniak, B. I. MacDonald, S. E. Watkins and P. Mulvaney, *Nano Lett.*, 2011, **11**, 2856–2864.

12 P. V. Kamat, *Acc. Chem. Res.*, 2012, **45**, 1906–1915.

13 B. K. Chen, S. Chang, D. Y. Li, L. L. Chen, Y. T. Wang, T. Chen, B. S. Zou, H. Z. Zhong and A. L. Rogach, *Chem. Mater.*, 2015, **27**, 5949–5956.

14 T. Kawawaki, H. B. Wang, T. Kubo, K. Saito, J. Nakazaki, H. Segawa and T. Tatsuma, *ACS Nano*, 2015, **9**, 4165–4172.

15 T. Niidome, Y. Akiyama, K. Shimoda, T. Kawano, T. Mori, Y. Katayama and Y. Niidome, *Small*, 2008, **4**, 1001–1007.

16 A. M. Smith, M. C. Mancini and S. M. Nie, *Nat. Nanotechnol.*, 2009, **4**, 710–711.

17 F. Wang, D. Banerjee, Y. S. Liu, X. Y. Chen and X. G. Liu, *Analyst*, 2010, **135**, 1839–1854.

18 Y. Il Park, K. T. Lee, Y. D. Suh and T. Hyeon, *Chem. Soc. Rev.*, 2015, **44**, 130s2–11317.

19 Y. G. Zheng, S. J. Gao and J. Y. Ying, *Adv. Mater.*, 2007, **19**, 376–380.

20 J. van Embden, A. S. R. Chesman and J. J. Jasieniak, *Chem. Mater.*, 2015, **27**, 2246–2285.

21 D. W. Deng, J. F. Xia, J. Cao, L. Z. Qu, J. M. Tian, Z. Y. Qian, Y. Q. Gu and Z. Z. Gu, *J. Colloid Interface Sci.*, 2012, **367**, 234–240.

22 A. J. Shuhendler, P. Prasad, H. K. C. Chan, C. R. Gordijo, B. Soroushian, M. Kolios, K. Yu, P. J. O'Brien, A. M. Rauth and X. Y. Wu, *ACS Nano*, 2011, **5**, 1958–1966.

23 I. Hocaoglu, M. N. Cizmeciyan, R. Erdem, C. Ozen, A. Kurt, A. Sennaroglu and H. Y. Acar, *J. Mater. Chem.*, 2012, **22**, 14674–14681.

24 B. H. Dong, C. Y. Li, G. C. Chen, Y. J. Zhang, Y. Zhang, M. J. Deng and Q. B. Wang, *Chem. Mater.*, 2013, **25**, 2503–2509.

25 T. Torimoto, T. Adachi, K. Okazaki, M. Sakuraoka, T. Shibayama, B. Ohtani, A. Kudo and S. Kuwabata, *J. Am. Chem. Soc.*, 2007, **129**, 12388–12389.

26 L. Li, T. J. Daou, I. Texier, T. K. C. Tran, Q. L. Nguyen and P. Reiss, *Chem. Mater.*, 2009, **21**, 2422–2429.

27 M. Sakamoto, L. H. Chen, M. Okano, D. M. Tex, Y. Kanemitsu and T. Teranishi, *J. Phys. Chem. C*, 2015, **119**, 11100–11105.

28 B. Tell, J. L. Shay and H. M. Kasper, *Phys. Rev. B: Solid State*, 1974, **9**, 5203–5208.

29 Y. T. Lim, S. Kim, A. Nakayama, N. E. Stott, M. G. Bawendi and J. V. Frangioni, *Mol. Imaging*, 2003, **2**, 50–64.

30 M. A. Langevin, T. Pons, A. M. Ritcey and C. N. Allen, *Nanoscale Res. Lett.*, 2015, **10**, 255.

31 D. C. Pan, L. J. An, Z. M. Sun, W. Hou, Y. Yang, Z. Z. Yang and Y. F. Lu, *J. Am. Chem. Soc.*, 2008, **130**, 5620–5621.

32 S. H. Chang, B. C. Chiu, T. L. Gao, S. L. Jheng and H. Y. Tuan, *CrystEngComm*, 2014, **16**, 3323–3330.

33 R. G. Xie, M. Rutherford and X. G. Peng, *J. Am. Chem. Soc.*, 2009, **131**, 5691–5697.

34 T. Torimoto, S. Ogawa, T. Adachi, T. Kameyama, K. I. Okazaki, T. Shibayama, A. Kudo and S. Kuwabata, *Chem. Commun.*, 2010, **46**, 2082–2084.

35 D. W. Deng, L. Z. Qu and Y. Q. Gu, *J. Mater. Chem. C*, 2014, **2**, 7077–7085.

36 M. A. Hines and G. D. Scholes, *Adv. Mater.*, 2003, **15**, 1844–1849.

37 Y. A. Yang, H. M. Wu, K. R. Williams and Y. C. Cao, *Angew. Chem., Int. Ed.*, 2005, **44**, 6712–6715.

38 G. Kanellis and K. Kampas, *Mater. Res. Bull.*, 1978, **13**, 9–16.

39 M. Quintero, R. Tovar, C. Bellabarba and J. C. Woolley, *Phys. Status Solidi B*, 1990, **162**, 517–521.

40 H. Z. Zhong, Y. Zhou, M. F. Ye, Y. J. He, J. P. Ye, C. He, C. H. Yang and Y. F. Li, *Chem. Mater.*, 2008, **20**, 6434–6443.

41 T. Torimoto, H. Nishiyama, T. Sakata, H. Mori and H. Yoneyama, *J. Electrochem. Soc.*, 1998, **145**, 1964–1968.

42 T. Uematsu, H. Kitajima, T. Kohma, T. Torimoto, Y. Tachibana and S. Kuwabata, *Nanotechnology*, 2009, **20**, 215302.

43 C. M. Hessel, D. Reid, M. G. Panthani, M. R. Rasch, B. W. Goodfellow, J. W. Wei, H. Fujii, V. Akhavan and B. A. Korgel, *Chem. Mater.*, 2012, **24**, 393–401.

44 R. C. Benson and H. A. Kues, *Phys. Med. Biol.*, 1978, **23**, 159–163.

45 W. W. Zheng, Y. Liu, A. West, E. E. Schuler, K. Yehl, R. B. Dyer, J. T. Kindt and K. Salaita, *J. Am. Chem. Soc.*, 2014, **136**, 1992–1999.

46 I. Moreels, K. Lambert, D. Smeets, D. De Muynck, T. Nollet, J. C. Martins, F. Vanhaecke, A. Vantomme, C. Delerue, G. Allan and Z. Hens, *ACS Nano*, 2009, **3**, 3023–3030.

47 C. Zhao, Z. Bai, X. Liu, Y. Zhang, B. Zou and H. Zhong, *ACS Appl. Mater. Interfaces*, 2015, **7**, 17623–17629.

48 X. Liu, G. B. Braun, H. Zhong, D. J. Hall, W. Han, M. Qin, C. Zhao, M. Wang, Z.-G. She, C. Cao, M. J. Sailor, W. B. Stallcup, E. Ruoslahti and K. N. Sugahara, *Adv. Funct. Mater.*, 2016, **26**, 267–276.

49 X. G. Peng, M. C. Schlamp, A. V. Kadavanich and A. P. Alivisatos, *J. Am. Chem. Soc.*, 1997, **119**, 7019–7029.